IIETA International Information and Engineering Technology Association
Advancing the World of Information and Engineering

Mathematical Modelling of Engineering Problems
Vol. 8, No. 4, August, 2021, pp. 597-610
Journal homepage: http://iieta.org/journals/mmep

Numerical Forced Convection Heat Transfer of Nanofluids over Back Facing Step and Through Heated Circular Grooves

Ali Hussein Abdulkarim[1], Muhammad Asmail Eleiwi[2], Tahseen Ahmad Tahseen[1], Eyub Canli[3*]

[1] Mechanical Engineering Department, University of Kirkuk, Kirkuk 36001, Iraq
[2] Mechanical Engineering Department, Tikrit University, Tikrit 34001, Iraq
[3] Mechanical Engineering Department, Technology Faculty, Selcuk University, Konya 42130, Turkey

Corresponding Author Email: ecanli@selcuk.edu.tr

https://doi.org/10.18280/mmep.080413

Received: 1 May 2021
Accepted: 11 June 2021

Keywords:
back facing step, CFD, heat transfer, laminar, nanofluid, temperature distribution

ABSTRACT

Backward facing step arrangement is a classical case for fluid dynamics and heat transfer research. It is well characterized and therefore, used for benchmarking. However, ongoing studies reveal that the geometry also provide advantages in industry, especially in combustion and burners. This work utilizes computational fluid dynamics to investigate a specific laminar back facing step flow heat transfer case. Aluminium oxide nano particles are considered as an additive to water base fluid, forming nanofluid with different volumetric concentrations. Laminar flow passes a back facing step and encounters three circular grooves at bottom surface. All surfaces are adiabatic except the grooves. Constant surface temperature applies to the grooves. According to the simulation results, a separation bubble after back facing step and a reattachment point occur. Grooves alter expected wake due to physical and thermal interference. Investigation parameters are nano-particle concentration and Reynolds number. Reynolds number changes between 10 and 250. Nano particle volume fraction percentage changes between 2 and 6 percent. Sectional heating downstream of the step poses interesting heat flux in the presence of Aluminium oxide nano-particle concentrations. There is a pseudo-linear relationship between parameters and heat transfer. Combined effects of enhanced thermal conductivity and secondary flow structures are seen. As expected, thermal convection increases as flow velocity and nano-particle concentrations increase. Heat flux and accordingly Nusselt number are highly affected from Reynolds number since flow structure changes dramatically. Also, direct proportion is seen between nano-particle concentration and enhanced convection.

1. INTRODUCTION

Today, certain tendencies towards enhancing heat transfer utilize nanoparticles to form nano-fluids and adding geometrical modifications. Another motivation of those tendencies is to achieve compactness which would lead to cost reduction and flexibility. These studies evaluate their proposition by considering heat transfer rates and pressure drop. In other words, trade-off between heat transfer and pressure drop due to design is considered. One of the key geometries is Back or Backward Facing Step (BFS). This geometry is feasible for benchmarking of numerical flow and heat transfer analysis means since it is well characterized. Nevertheless, it is also encountered in industrial applications such as burners and heat exchangers. Separation bubble downstream of the step, wake and reattachment point have been widely used for benchmarking studies of various Computational Fluid Dynamics (CFD) works and experimental apparatuses. Also, shear layers and mixing phenomena are complex enough to investigate and test higher order approaches. Together with nanofluids, BFS poses potential for new outcomes in terms of fluid dynamics and heat transfer. When combined with further geometrical alterations, specific cases become attractive to be investigated. Therefore, this work focuses on laminar forced convection heat transfer due to altered flow of BFS, nano particle addition, geometrical modifications, and partial heating.

Literature survey has been grouped in four categories, i.e., flow, heat transfer, mixing for combustion and nano-fluid research, respectively.

Karasu [1] used BFS for benchmarking k-ϵ turbulence model with standard wall functions. Author identified three regions; a dynamic swirling wake region; a shear flow towards reattachment point; and a stagnation line. It is stated that the turbulence model predicts a shorter and thinner separation bubble downstream of BFS. Although the reason for misprediction of reattachment length by the turbulence model is attributed to characteristic of the model by the author (missing turbulence non-equilibrium), it is thought that standard wall functions and mesh structure might lead to such results. Yang et al. [2] also benchmark k-ϵ turbulence model and its variations with BFS. Variations contain linear and non-linear model versions. Authors emphasize effectiveness of non-linear k-ϵ turbulence models over standard model. However, it is thought that complexities are also increasing with nonlinear models. Almohammadi [3] benchmark 14 turbulence model by reattachment point of BFS turbulent flow. Wang et al. [4] used Large Eddy Simulation (LES) CFD model in order to assess its capabilities by using it with a BFS flow. Although reattachment point is found very close to the

experimental value, skin friction profile and streamwise velocity profiles downstream of the step are not very accurate considering the computational cost of the LES. Especially recirculation zone simulated values are different than experimental ones. Vogel [5] cite Vogel and Eaton for experimental results of flow over BFS. Mean skin friction coefficient downstream of the step marks recirculation region. Also, streamwise velocity profiles show reattachment point. Peak values of turbulence intensity were measured at slightly upstream of the reattachment point. Turbulence mixing in the separated free shear layer is reported to be very strong. A laminar boundary layer, thickening towards the recirculation bubble is detected, upstream of reattachment point. Assam et al. [6] focus on rarefaction and non-continuum effects on the flow and heat transfer for various geometries including BFS. Wall slip velocities and non-equilibrium occur due to rarefaction which is not only due to low density gas flow but also due to nano scale channel characteristic length. Flow Mach number changes dramatically from subsonic (0.65) to almost zero. Relatively high Mach number values are seen at the cross section close to the step edge. Mach numbers with very small values are seen close to wall as expected. The recirculation zone is quite small and reattachment length is relatively and actually very short. In the flow related review part, the paper of Erturk [7] is thought to be the most relevant numerical study. Author used very fine mesh and very small residual limits in order to investigate BFS laminar flow between 100 and 3000 Reynolds number (Re). According to the study, Re=800 is seen as a limit for incompressible steady laminar BFS solution. The steadiness here is about characterization of wake flow in terms of same geometrical values and patterns. After Re=800, bifurcation occurs. However, the author managed to solve up to 3000 Re by intensifying mesh number, using very low residual limits and stream function-vorticity formulation for finite difference solution method. The paper can be criticized since turbulence could be considered after Re 2000. Nevertheless, reattachment points, recirculation sizes are given in detail in the paper. It is stated that recirculation bubbles grow linearly with Re. Two bifurcations Re interval are also identified in the paper. Five times step height is recommended for inlet channel length. It should also be noted here that more than one separation bubbles occur at bottom and upper surfaces of the calculation domain. Separation bubbles elongates and increase in number as Re increases. In the paper, author refer to experimental work of Armaly et al. [8]. In that work, authors provide very detailed flow results of BFS between Re 70 and 8000. Authors also state that turbulence transition starts from Re 1200. BFS reattachment length growing with Re is stated that as not linear as symmetrical sudden expansion. Nowruzi et al. [9] used energy gradient method for simulating BFS laminar flow. Authors provide an excellent literature survey, and the flow related part are very important in respect of the present paper. They state that the shear layer instability downstream of the BFS mainly originated from the step edge and its proximity. Zhu et al. [10] studied supersonic BFS flow experimentally. This type of flow has very short reattachment. There are shock waves due to impingement of the flow at the reattachment, and redeveloping boundary layer under the shock wave. Guo et al. [11] investigated hypersonic flow over BFS numerically by Direct Simulation Monte Carlo (DSMC) method for near space engineering. They identified very different behaviour as altitude gets high. They do not only investigate altitude but also jet perturbation strategies of the flow. One such work, but for small Re in incompressible range is reported by Dejoan and Leschziner [12]. Authors used Large Eddy Simulation (LES) in order to perturbed turbulent BFS flow. They inform that recirculation is smaller for perturbation and shear layer is flapping and this flapping phenomenon is called shedding instability. There are also experimental works on BFS with perturbation in transitional or turbulent flows [13]. Authors report 20% reduction in reattachment length due to perturbation jet by phase averaging results with particle image velocimetry. In another work, BFS step is modified with an inclination for turbulent flow and several numerical approaches including finite elements and finite volumes are compared [14]. Nevertheless, authors state that finite volumes method with Reynolds Stress model is favourable against finite elements model. Choi and Nguyen [15] used Reynolds Averaged Navier Stokes (RANS) and LES in order to numerically investigate BFS turbulent flow with step inclination angles. They stated that reattachment length is almost constant after Re=15000 even with inclination angles higher than 30°. According to literature review of BFS flow, it is seen that laminar and turbulent recirculation zones are different. Also, there can be more than one recirculation zone at counter surfaces downstream of BFS for laminar flow. Laminar BFS flow is well characterized up to Re 800 by steady analyses. Almost all works viewed about flow analyses reveal that BFS is not only a benchmark tool but also a geometry for heat transfer and flow mixing in industrial applications. The present paper does steady flow analyses up to Re=250, therefore it is proper according to the literature. A single wake with relatively short reattachment point is expected.

In the second part of literature survey, heat transfer analyses are viewed for BFS flow. Rouizi et al. [16] studied modal identification method in order to reduce CFD cost for laminar forced convection BFS flow. Authors claim 720,000 times faster computation by the reduced model. Heating was done at the upstream surface of the step. In another work, this time in experimental analysis, downstream of laminar BFS is heated [17]. Authors search for effects of pulsating flow and surface corrugation where heating is done. They state that pulsating enhances heat transfer up to a certain Strouhal number, but corrugation is found ineffective. In fact, authors say that heating surface corrugation may lead to worse heat transfer. Coskun et al. [18] utilized OpenFOAM CFD in order to investigate effects of suction and injections on laminar BFS heat transfer. Re was picked as 400 constant value while 19 different cases were arranged by suction and injection scenarios. Kumar and Dhiman [19] modified laminar BFS flow by means of a circular cylinder in order to enhance convective heat transfer. They report about 2.5 times increase in convective heat transfer by altering recirculation of laminar BFS flow. Resulting pressure drop increase is given as 37% high due to the presence of the circular cylinder. Most of laminar BFS heat transfer is investigated by 2D CFD but there are 3D cases where side walls and temporal resolution exits [20]. Authors detect a second Nusselt number (Nu) peak at the middle plane of 3D BFS due to flow instability after Re=1000. Xie and Xi [21] investigate transitional Re numbers for laminar BFS heat transfer with transient CFD and fine mesh. They also show flow instability of transitional flow over Re=1000 and its effects on heat transfer. They show that there is a single Nu peak below Re=1000 and its position is not changing with time. On the other hand, there are two Nu peaks at Re=1000 and its location changes with time. Xie et al. [22] investigate transitional laminar BFS heat transfer and report

flow instability yielding three Nu peaks. Boruah et al. [23] place baffles downstream of BFS for altering laminar flow separation and try to enhance heat transfer while calculating entropy generation due to the baffles. Re is fixed at 100 while Richardson number changes. Baffle configuration changes and they report different entropy generation rates according to baffle size and configuration. Also, they state that recirculation zone has less entropy generation comparing to the reattachment point. In another numerical study, authors investigate nano-particle addition, flow pulsation and surface corrugation as parameters for laminar BFS heat transfer enhancement [24]. All the surfaces except corrugation surfaces are taken adiabatic. According to their results, surface corrugation decreases, and nano-particle addition increases heat transfer. Authors also used Proper Orthogonal Decomposition and Artificial Neural Network. This relatively recent work can be regarded as a consequent report of a series [25-28]. Actually, pulsating laminar flow BFS heat transfer can be tracked to earlier dates [29]. Authors emphasize Nu number increase by pulsation. On the other hand, most of above reviewed studies assume that there are not side walls or side walls are distant. Juste and Fajardo [30] investigate a narrow channel BFS flow heat transfer. They used CFD and experimental means, i.e., Moire deflectometry. Aspect ratio for the side walls is 4. They conclude that low aspect ratio and accordingly side walls lower heat transfer for the beginning of transitional regime about Re=1200. Of course, there are studies with turbulent flow heat transfer. Experimental works, in general, contain very few examples of laminar BFS heat transfer. However, similar geometries that can be used by resemblance exist [31]. Li et al. [32] investigated perturbated turbulent flow over BFS. They reported shortened recirculation bubble and local heat transfer enhancement. Vogel et al. [5] identified fluctuating skin friction in near proximity of the wall that govern heat transfer rate in the separation. They also mentioned that two or three step heights is sufficient for conventional Reynold's analogy of the heat transfer rate after reattachment. Chen et al. [33] investigated effects of step height for turbulent BFS heat transfer. They state that peak Stanton number gets smaller as step height increases. Amiri et al. [34] used BFS in order to show effects of graphene nano particles on heat transfer effectiveness of a fluid mixture in turbulent regime. Authors found heat transfer enhancement by the comparison of BFS heat transfer values of water and the mixture. Mittal et al. [35] stress intrusion effects of flow measurement on heat transfer calculations of turbulent BFS heat transfer and propose an analogy between heat and mass transfer. Authors used naphthalene since they can measure the mass transfer without intrusion and then detected an analogy coefficient of 0.692. Hilo et al. [36] investigated addition of two nano-particle types into ethylene glycol fluid for turbulent BFS heat transfer by experimental means. They detected heat transfer enhancement. One interesting phenomenon is slip flow that can be observed by compressible gases flowing in micro and nano channels and pipes and this phenomenon affects heat transfer [6]. Authors found significant differences between tried models and suggested that slip friction changes prediction accuracy depending on cases. Hilo [37] used both experimentation and CFD in order to investigate heat transfer downstream of a backward facing step while bottom side of the channels have corrugation geometries inwardly to the flow. Several corrugation geometries are assessed. It is worth to mention two review studies here which give numerous examples of BFS heat transfer research [38, 39]. There is also another geometrical case called Forward Facing Step (FFS). Although separation bubble and wake flow are different, case setups have similarities. Therefore, some examples can be given [40-44]. A second FFS or additional blockage geometries can be inserted as a passive control geometry of the first step [41, 43]. Finally, three example studies that illustrate several different geometries partially involving step geometries and related heat transfer phenomena [45-47].

BFS geometry can also be used for industrial purposes. One prominent example is being a mixing device for combustion. For instance, Yang et al. [48] experimentally investigate two types of micro-combustors that burns hydrogen as fuel. One micro-combustor has BFS, and it was compared with the other one that has straight shape. The proposed BFS micro-combustor is found favorable over the other one. Khandelwal et al. [49] present three step BFS that may be encountered very few in the literature, if none is encountered, as a micro channel combustor for flame stabilization. Choi et al. [50] characterized flame of premixed turbulent air fuel mixture after a BFS combustor. They used flow visualization and therefore present a solid visual data. Four flame modes are identified. BFS is given as an intrinsic part of the combustor. A very interesting and recent work is reported about scramjets and BFS geometry is examined in terms of combustion efficiency and pressure drop [51]. They examined geometrical parameters of BFS. Aabid and Khan [52] review BFS geometry in respect of convergent divergent nozzle that is used in industry.

Final part of the literature survey is composed of nanoparticles as additives to heat transfer fluid mediums. Total mixtures are called nanofluid for enhanced heat transfer performances. Some instances are already mentioned in previous BFS heat transfer paragraph. Ghasemi and Razavi [53] used finite volume lattice-Boltzmann method in order to simulate CuO-H_2O nanofluid heat transfer. Authors used BFS to validate their simulation and also detect important heat transfer enhancement by the nanoparticle addition. Hernandez et al. [54] shows potential improvement points in conventional solar distillation process by nano material including nanofluids. Amorim Neto et al. [55] utilized silver and titanium dioxide nano particles to have a nanofluid in solar heating system. Authors stated a specific molar concentration amount of nanofluid mixture for better thermal performance. Khodabandeh et al. [56] also used silver nano particles with similar percentages to Amorim Neto et al. [55] for obtaining nanofluid as heat transfer medium in heat exchangers. Authors reported heat transfer enhancement due to silver nanofluid utilization. A very common nanofluid by mixing of copper oxide and water is numerically investigated with a relatively interesting configuration by Selimefendigil and Chamkha [57]. Authors reported very high heat transfer enhancement with the increase of nanofluid concentration. Abedalh et al. [58] mixed two different nano particles with pure water in order to have a mixture nanofluid concentration for experimental assessment of thermal performance of the mixture nanofluid in a backward facing step test rig. The experimental work and mass fractions between 1 to 3% makes report very attractive for CFD validation. Heat transfer enhancement is given as 14% while pressure drop increases 4%. Abed et al. [59] reports several nanofluids for partial and nonuniform heating of circular cross-section channels. The work uses CFD in order to simulate extreme cases such as high temperatures, viscosities, and thermal radiation. Silicon Dioxide is found prominent

among other nanofluids. Ahmed et al. [60] used Al_2O_3 for enhancing thermal performance of crossflow tube bank heat exchangers. In a similar case, Ahmed et al. [61] use same nanofluid for shifting phase of sinusoidal wavy fins. Volume fraction of the nanofluid changes between 0 and 5%. Ajeel et al. [62] benchmark four different nanofluids, i.e., ZnO, Al_2O_3, CuO, and SiO_2, via CFD in a corrugated channel. Again, SiO_2 is found favourable, among others. However, possible downfalls or negative sides are not mentioned. Hechavarria et al. [63] proposed a new way of measuring nanofluid thermal conductivity by using a photothermal technique. Rocha et al. [64] reported a review about preparations of nanofluids. It is interesting not to encounter any negative report about nanofluids. This tendency of scientific literature, i.e., reporting good results but not presenting bad ones or relatively insignificant ones, is being debated. However, in the meantime, it is best to keep up with heat transfer enhancement studies with nanofluids.

In this work, three half circle grooves are placed downstream of a BFS. Laminar nano fluid flow passes through the geometry. Al_2O_3 nano particles are selected with three different volumetric concentrations. Reynolds number is also changed in laminar interval. All surfaces except the surfaces of the grooves are adiabatic. Constant surface temperature boundary condition is applied to the surfaces of the grooves. CFD is utilized in order to have velocity, pressure, and temperature distribution in the domain. Results are evaluated in terms of convective heat transfer.

2. THEORETICAL APPROACH AND METHOD

The two-dimensional numerical calculation domain is given in Figure 1 schematically. This geometry is basically a BFS having three additional half circular grooves downstream of the step. Flow inlet is the left vertical edge of the geometry and flow outlet is the right vertical edge of the geometry. All edges of the calculation domain are set as wall except inlet and outlet. Walls are adiabatic, meaning that no heat is transferred through walls except the three grooves. Three circular grooves are held at 323 K constant temperature. Flow enters to calculation domain with 293 K temperature value. Therefore, heat is transferred from grooves to the fluid. Accordingly, the only heat transfer mechanism is fluid forced convection.

The BFS that is visible in Figure 1 creates a recirculation zone downstream of the step. This recirculation zone has a shear layer boundary with the upper side of the flow. A complex interaction between recirculation zone and upper part is expected through shear layer due to high instability potential of the layer. Recirculation zone, reattachment point, and shear layer also interact with grooves, creating more mixing and thermal convection. Convection is the right term here since advection by itself is not enough for defining complete heat transfer. Especially nano particles contribute to the thermal diffusion capacity of the fluid, and this leads to considerable contribution of thermal diffusion to convection. Convection is a combination of thermal advection and diffusion. Three points, i.e., x1, x2 and x3 are marked in Figure 1, showing special locations for cross-stream traverse profiles.

Problem is solved by Ansys Workbench by several sub systems. Geometry was constructed in Design Modeler. Mesh was prepared by Ansys meshing. Fluent software was used for numerical solution. A very fine mesh was used in order to evade mesh independency studies. This mesh is illustrated in Figure 2. Ultra-fine structure of the mesh leads to pseudo quadrilateral elements for almost complete flow domain. Inflation function is used for heat source surfaces. The necessity of inflation may be argued here since general mesh element sizes small enough for close proximity of the heat source walls. Nevertheless, inflation function yielded a structured and organized mesh structure near heat source walls. Total 204,691 elements were obtained after mesh generation. This group of mesh elements have 206,600 nodes on them. Ten inflation layers stack on heat source walls. First layer thickness is 0.05 mm and grow rate was set to 1.01.

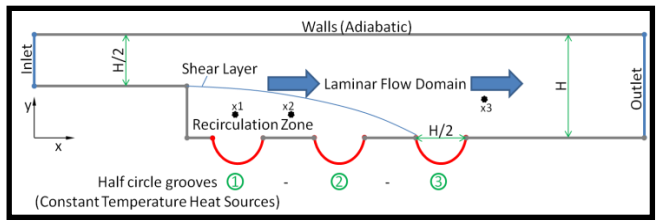

Figure 1. Schematic drawing of the numerical domain

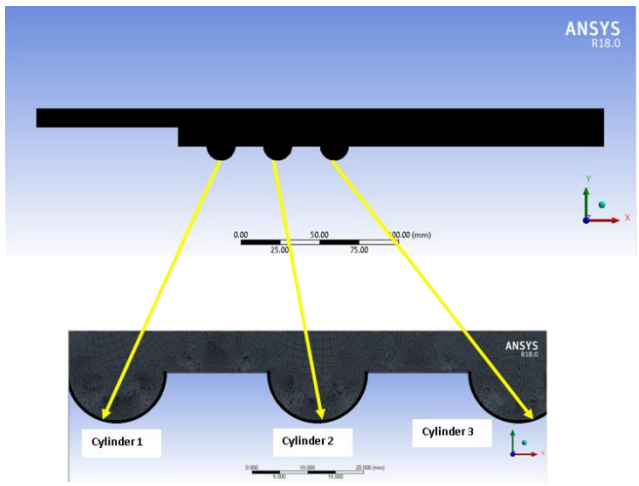

Figure 2. Mesh structure of the domain

Inlet boundary condition was set to "Velocity Inlet" with axial velocity component values for Re=10, 50, 100, 150 and 250. Outlet boundary condition was set to "Pressure Outlet" with 0 Pa gauge pressure value. All walls except groove surfaces were set to no slip wall boundary condition with 0 heat flux. Groove surfaces were also set to no slip wall, but their surface temperature values were set to constant 323 K. Properties of working fluids are given in Table 1. Volume fraction percentages of Al_2O_3 nano particles are shown with φ symbol.

Table 1. Thermo-physical properties according to nanoparticle concentration

	ρ	C_p	μ	k
Water	998.2	4182	0.001003	0.613
φ=2%	1057.63	3925	0.001053	0.648
φ=4%	1117.07	3969	0.001103	0.686
φ=6%	1176.51	3490	0.001153	0.724

Values in Table 1 are calculated with below equations. Same convention of equations is viewed in literatures [65, 66]. The equations are for density, specific energy, viscosity, and thermal conductivity, respectively. Symbols and subscripts are

explained in Nomenclature section. Constant property values were selected from tables for 293 K inlet temperature of the fluid mixture. Calculated values in Table 1 remains constant with changing temperature during heat transfer. This is not a problem since temperature difference is maximum 30 K and differences in property values for such a temperature difference can be ignored.

$$\rho_{nf} = (1-\varphi)\rho_{bf} + \varphi\rho_p \tag{1}$$

$$(\rho c_p)_{nf} = (1-\varphi)(\rho c_p)_{bf} + \varphi(\rho c_p)_p \tag{2}$$

$$\mu_{nf} = \mu_{bf}(1+2.5\varphi) \tag{3}$$

$$k_{np} = \frac{k_p + 2k_{bf} + 2(k_p - k_{bf})\varphi}{k_p + 2k_p - 2(k_p - k_{bf})\varphi} k_{bf} \tag{4}$$

After defining boundary conditions and fluid properties, the next step is deciding solver settings. A steady heat transfer case is aimed to be numerically solved. Therefore, solver was set to steady viscous-laminar and energy solution. Relevant conservation equations in vectoral form are given between Eqns. (5)-(7) and then their expanded versions are given between (8)-(11) [67]. Details of derivation differential elliptic forms of the governing equations from vector forms are explained in the given reference [67]. Eq. (5) is conservation of mass. Conservation of momentum is indicated in Eq. (6) by vectoral operators. Eq. (7) shows conservation of energy. Expanded continuity, x momentum, y momentum and energy equations are given subsequently and respectively.

$$\frac{\partial \rho}{\partial t} + \nabla\bullet[\rho \mathbf{v}] = 0 \tag{5}$$

$$\frac{\partial}{\partial t}[\rho \mathbf{v}] + \nabla\bullet\{\rho \mathbf{v}\mathbf{v}\} = \mathbf{f} \tag{6}$$

$$\begin{aligned} &\frac{\partial}{\partial t}(\rho e) + \nabla\bullet[\rho \mathbf{v} e] \\ &= -\nabla\bullet\dot{q}_s - \nabla\bullet[\rho \mathbf{v}] + \nabla\bullet[\boldsymbol{\tau}\bullet\mathbf{v}] + \mathbf{f}_b\bullet\mathbf{v} + \dot{q}_V \end{aligned} \tag{7}$$

$$\frac{\partial U}{\partial X} + \frac{\partial V}{\partial Y} = 0 \tag{8}$$

$$\left(U\frac{\partial U}{\partial X} + V\frac{\partial U}{\partial Y}\right) = -\frac{\partial P}{\partial X} + \frac{1}{\mathrm{Re}}\left(\frac{\partial^2 U}{\partial X^2} + \frac{\partial^2 U}{\partial Y^2}\right) \tag{9}$$

$$\left(U\frac{\partial V}{\partial X} + V\frac{\partial V}{\partial Y}\right) = -\frac{\partial P}{\partial Y} + \frac{1}{\mathrm{Re}}\left(\frac{\partial^2 V}{\partial X^2} + \frac{\partial^2 V}{\partial Y^2}\right) \tag{10}$$

$$\left(U\frac{\partial \theta}{\partial X} + V\frac{\partial \theta}{\partial Y}\right) = \frac{1}{\mathrm{Re}\,\mathrm{Pr}}\left(\frac{\partial^2 \theta}{\partial X^2} + \frac{\partial^2 \theta}{\partial Y^2}\right) \tag{11}$$

Variables in Eqns. (8)-(11) are dimensionless. This type of presentation is better for explanation. Results section graphics and tables are provided with results having dimensions. Length variables are made nondimensional by channel height, i.e., $X = \frac{x}{H}$, $Y = \frac{y}{H}$. Velocity variables are made nondimensional by inlet velocity value, i.e., $U = \frac{u}{u_{in}}$, $V = \frac{v}{v_{in}}$. Re number, Prandtl number (Pr) and Peclet number (Pe=Re·Pr) are defined below. These definitions are consistent with literature [68].

$$\mathrm{Re} = \frac{u_{in} \cdot H \cdot \rho}{\mu} \tag{12}$$

$$\mathrm{Pr} = \frac{\mu \cdot c_p}{k} \tag{13}$$

$$Pe = \mathrm{Re}\cdot\mathrm{Pr} = \frac{u_{in} \cdot H \cdot \rho}{\mu}\frac{\mu \cdot c_p}{k} = \frac{u_{in} \cdot H \cdot \rho \cdot c_p}{k} \tag{14}$$

Re number and Pe number intrinsically appear in the governing equations as natural independent parameters. This reduces parametrical research to changing just Re and Pe. In this work, Re is arranged by inlet velocity and Pe is arranged by nano particle volume fraction ratio. Temperature is normalized as $\theta = \frac{T-293}{323-293}$. Pressure nondimensionalization was done again with inlet velocity but by kinetic energy formulation, i.e., $P = \frac{p}{\rho\cdot(u_{in})^2}$. It is worth to repeat here that nondimensionalization is given here for only explaining numerical frame. Results of this work are given with dimensions.

Pressure velocity coupling was done according to COUPLED algorithm. Spatial discretization was done with second order upwind scheme for momentum and energy equations. Pressure equation discretization was done according to PRESTO! scheme. Least Squares Cell Based interpolation for gradients was utilized despite the fact that mesh elements have pseudo-quadrilaterals shapes. This is thought as a precaution for better numerical accuracy and stability.

Results are given mostly by primitive variables such as velocity magnitudes and temperatures. Those primitives are given with graphical representation and with cross-stream profiles at three predetermined locations. Predetermined locations are shown in Figure 1 as x1, x2 and x3. On the other hand, Nusselt number (Nu) as a dimensionless indicator of convection heat transfer is also given. The definition of Nu is written below in Eq. (15). Eq. (16) shows average Nu. Below equations are commonly used in the literature [68].

$$Nu_x = \frac{h_x H}{k} = \frac{-\left(\frac{\partial T}{\partial y}\right)H}{T_W - T_\infty} = -H\frac{\partial T}{\partial y} \tag{15}$$

$$\overline{Nu} = \frac{1}{dA}\int Nu_x dA \tag{16}$$

Considering presented method given above, a steady heat transfer CFD calculation procedure was implemented. Obtained results are given with graphical and tabular means in the next section.

3. RESULTS AND DISCUSSION

The logical flow in presentation of the results adopt deduction from final result towards primitives. Therefore Figure 3 is given in order to show average Nu based on Re and nano particle volume fraction ratios.

Average Nu increases with increasing Re, which is actually

an expected phenomenon. Increase proportionality is linear up to Re=150. After Re=150 to 250, rate of increase is decreasing. This trend can be reduced to and represented by a second-degree polynomial regression curve. This average Nu behaviour depending on Re is almost same for all fluids, i.e., base fluid and nanofluids. Increasing nano particle fraction in the base fluid increases average Nu number absolute value for a certain Re. This increase based on nanoparticle fraction seems linearly proportional. However, the slope of increase seems to be higher for higher Re number values. It is known that nano particle amount in the fluid changes the thermal diffusion ability of the mixture. Eq. (4) already shows this fact. However, it is seen from Figure 3 that thermal diffusion increase by the increase in conduction coefficient yields comparable amount of effect considering the pure advection case. Interestingly, this is valid for higher Re where advection is getting stronger. This suggests that thermal diffusion greatly supports advection emerging from fluid motion in the vicinity of the grooves, leading to higher convection coefficient and higher average Nu. It is also anticipated that more nano particle fraction would result in higher Nu and heat transfer rate, which is the aim of future work. The nonlinear increase of Nu with increasing Re suggests that increasing mass flow rate of the fluid mixture has significant change of flow structures. However, as Re value grows, the change in flow structures is somehow lower. These evaluations are due to the fact that thermal convection is mostly rely on advection emerging by means of the flow. Increasing thermal convection means increasing heat transfer. When the increase is due to Re increase, which also indicate higher flow rates, heat transfer is enhanced by two factors. On the other hand, when thermal convection coefficient is almost constant for increasing Re, this means heat transfer increases with only by increasing flow rate. Although we have information about effects of Re and φ on average Nu and heat transfer by Figure 3, we have no idea about how grooves and BFS act on these results. Therefore, temperature distribution along the calculation domain should be examined.

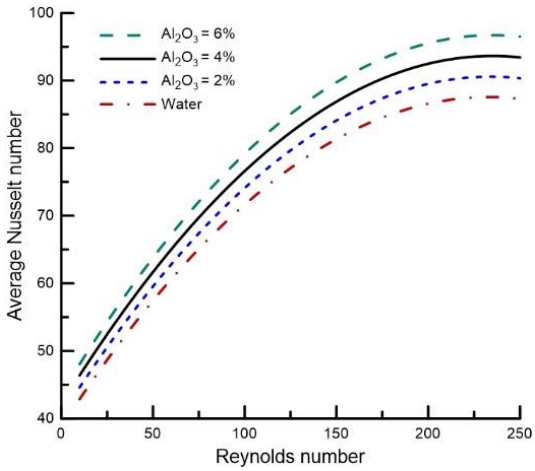

Figure 3. Average Nu depending on Re and φ

Temperature distribution in graphical form is given by means of two figures. Figures 4 and 5 are given in order to show temperature distribution in the calculation domain according to Re number and nanoparticle volume fraction percentage. Figure 4 is for Re numbers from 10 to 100. Figure 5 is for Re numbers 150 and 250. Figures 4 and 5 should be evaluated together. Qualitative comparison of Figure 4 and 5 suggests that temperature distribution intensity change its location from latter part of the computational domain to the near region of step edge as Re grows bigger. Less flow motion at small Re leads to thermal diffusion dominant heat transfer. Therefore, fluid masses with increased temperature are swept by the flow mildly, creating a high temperature field at the downstream of the grooves in Figure 4. However, in Figure 5, mixing phenomenon due to the step increases the temperature in the separation bubble and then temperature drops as the fluid mixes with downstream part of the domain. Nevertheless, quantitative assessment with the contours in respect of nano particle fraction is very hard to achieve. By continuing evaluations in an order from minimum Re value to maximum value respectively, first thing to be emphasized here is the weak effect of nano particle volume fraction percentage on the temperature distribution. Nano particles have very small effect on Re number since inlet velocity is given constant for a certain Re arrangement. For instance, inlet velocity was set to 0.000837 m/s to have Re=10. However, nano particle addition changes density and viscosity of the fluid slightly. Therefore 2, 4 and 6% nano particle volume fractions modify Re respectively as given in the following: 10, 10.08, 10.17, 10.24, 50, 50.44, 50.86, 51.24, 100, 100.88, 101.72, 102.48, 150, 151.26, 152.52, 153.67, 250, 251.9, 253.99 and 255.91. This small effect on Re is ignorable. Therefore, flow is not altered by the nano particle addition. This statement will be justified with upcoming figures. However, no significant changes are visible in temperature distribution due to nano particle volume fraction changes. Only visible change is in parts near outlet region with small temperature gradient differences. Those small differences also vanish with increasing Re. It can be concluded here that the tried volume fractions of nano particles do not alter Pr number and accordingly Pe number leading to very small changes in temperature distribution. The reason of increasing average Nu numbers is then due to the amount of transferred heat. Heat transfer amount can be higher for constant temperature difference with lower thermal resistance. Accordingly, nanofluids have lower thermal resistances and higher thermal conduction coefficients realizing higher average Nusselt numbers. On the other hand, Re dramatically changes temperature distribution. For Re=10, the dominant mechanism is almost pure diffusion. It resembles to mass transfer of naphthalene or smoke under weak wind. A recirculation zone occurs at Re=50. This recirculation zone at Re=50 merges with the circular groove 1 and creates a relatively high temperature zone. It is interesting to see heating towards upstream through the recirculation zone and shear layer. This is due to relatively slow movement of the recirculation zone, enabling effective heat diffusion. Of course, these evaluations will be justified by velocity distribution figures. Remaining two circular grooves at Re=50 continue to contribute diffusional heat transfer mechanism. Relatively moderate temperatures are seen in close proximity of the bottom wall due to no slip boundary condition which reduces flow speeds greatly and leads to increased temperature values due to diffusion. Most of the flow seems not to be affected in terms of temperature. When Re reaches to 100 value, moderate temperature zone starting from the edge of the step reaches to second groove. This weakness the downstream diffusion layers and they become thinner. At this point, most of the heat is transferred to bulk flow by means of the recirculation zone and shear layer. This tendency continues with Re=150 and 250 by making downstream diffusion layers almost vanish. Thermal moderate temperature zone that resembles to the

recirculation zone reaches to third circular groove at Re=250. It is therefore thought that BFS thermal convection ability is increases with increasing Re. Nano particle fractions maintains temperature distribution almost unchanged for higher heat transfer. With constant heat flux, one would expect smaller temperature gradients with increasing nano particle volume fractions. The final evaluation about temperature distributions can be done by evaluating thermal convection coefficients at circular groove surfaces. Therefore Table 2 is given below.

Table 2. Thermal convection coefficients at circular grooves (units in W/m2·K)

	φ=0%			φ=2%			φ=4%			φ=6%		
u_{in}	1	2	3	1	2	3	1	2	3	1	2	3
0.000837	50.08	39.02	34.55	52.09	40.58	35.88	54.13	42.14	37.22	55.9	43.59	38.5
Average		41.22			42.85			44.5			46.01	
0.004185	71.94	59.07	51.63	74.49	61.44	53.73	77.01	63.87	55.85	79.52	66.36	58.01
Average		60.88			63.22			65.57			67.97	
0.00837	74.94	68.27	65.96	76.39	71.47	68.42	77.95	74.65	70.94	79.71	77.76	73.49
Average		69.72			72.09			74.51			76.98	
0.01255	52.33	117.51	73.76	54.06	121.52	76.2	55.83	125.55	78.62	57.62	129.6	81.09
Average		81.2			83.93			86.67			89.44	
0.0209	44.07	66.85	151.61	45.51	68.77	157.44	46.97	70.74	163.33	48.48	72.76	169.12
Average		87.51			90.57			93.68			96.78	

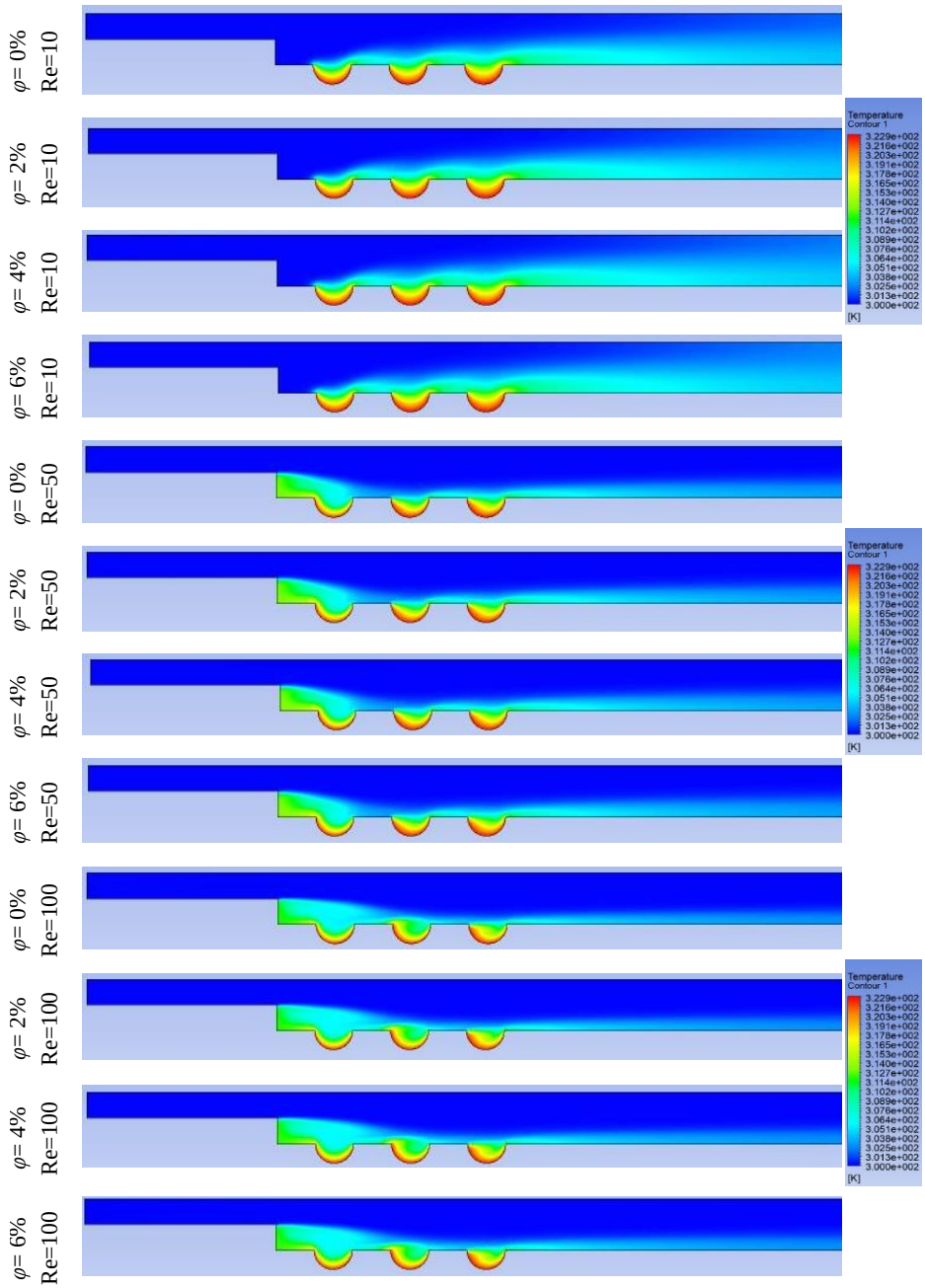

Figure 4. Temperature distribution in the calculation domain according to Re=10, 50, 100 and nano particle volume fraction ratio

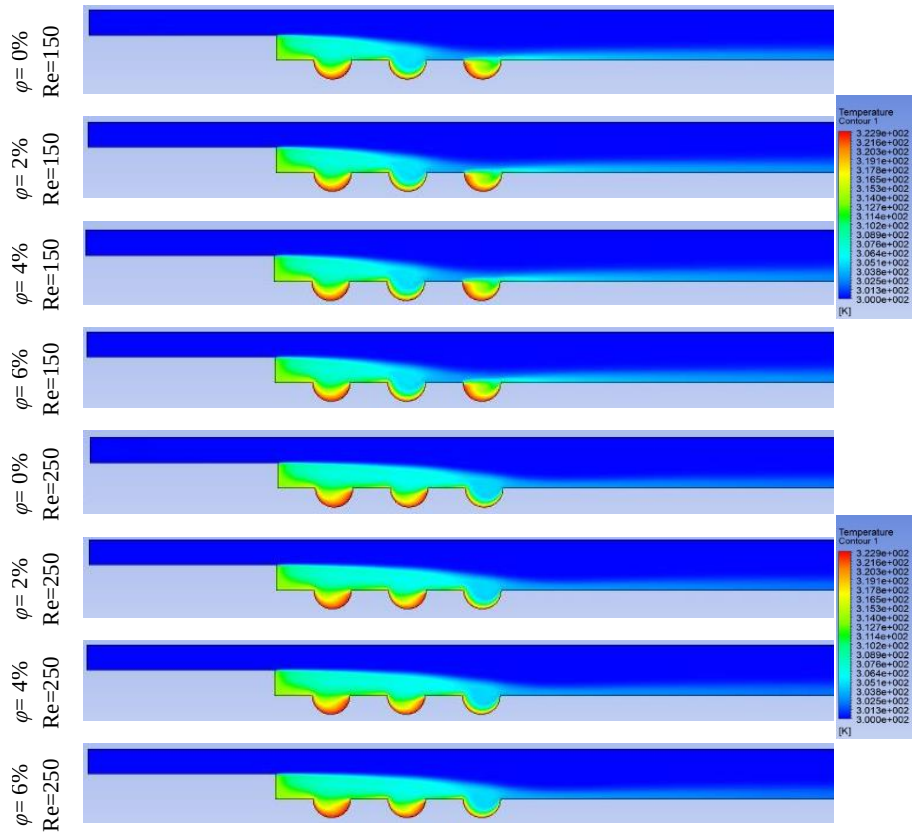

Figure 5. Temperature distribution in the calculation domain according to Re=150, 250 and nano particle volume fraction ratio

Since thermal convection coefficient is not only depending on temperature gradient but also to the heat flux to be transferred to the bulk flow, effects of both Re and nano particle volume fraction can be seen in Table 2. Especially average thermal convection coefficient values give parallel results to Figure 3. However, it is clearly seen that Re shifts position of maximum groove thermal coefficient values from first groove to the next one and then the last one. For Re=10, the first groove has the highest thermal convection coefficient value. This situation continues up to Re=150 with being equalized between first and second groove values. At Re=150, the second groove has the highest thermal convection coefficient. For Re=250, the highest thermal convection coefficient values are seen in third circular groove. BFS flow recirculation zone, shear layer and reattachment point interact with flow in grooves leading to very different thermal convection behaviour. This result should be emphasized in order to state that certain Re numbers yield domestic heat transfer enhancements near reattachment points. Of course, all these evaluations are based on heat transfer results, and they need to be justified by flow data. Three points are marked in Figure 1 showing velocity profile locations. These profiles are given in Figure 6 in order to show differences based on Re. Re=10 velocity profiles are almost not affected from grooves. This explains the pure diffusion condition at Re=10. However, starting from Re=50, upper part of the channel shows great increase in maximum velocity magnitude while bottom part is affected from the groove geometries. The peak velocity magnitude points have a slightly shift to positive y direction with increasing Re. This is due to compensating mass flux deficit because of the groove geometries. It is also seen that flow rapidly redevelop and have parabolic profile easily for all Re numbers. Re=10 can be regarded as an exception since relatively long ranges may be needed for this low value Re. The main differences in the velocity profiles given in Figure 6 a, b and c are due to different flow-boundary interactions due to the existing shear phenomena rather than the nano particle concentrations. Since gravity is ignored, heat dissipation and diffusion causing temperature differences in the flow are not altering the flow field. Therefore, velocity distribution is only affected by the shear between fluid particles and solid boundaries. As Re grows bigger values, momentum transfer changes the velocity distribution by the interactions between the flow and the solid surfaces. The effects of the groove shapes are apparent in the velocity profiles. Nevertheless, the best way to evaluate velocity field is to give distribution graphics similar to the temperature ones. Therefore Figure 7 is given, showing the velocity distribution contours for tried Re and nano particle volume fraction percentages. Figure 7 is evaluated in terms of flow field. At Re=10, 4 small recirculation zones or “stagnant” zones are apparent. The first zone is next to the step, other three is in the grooves. Considering the temperature distribution graphics, heat is dissipated from surfaces of grooves by diffusion towards downstream via the core flow region. There is almost no stagnant connection between those zones. The only connection is through laminar flow layers. Maximum velocity greatly reduces after expansion. At Re=50, the first recirculation zone grows and reach to the first groove by its reattachment point. A thermal diffusion link is created in the first recirculation zone considering both temperature and velocity distributions. The first recirculation region can reach into depths of the first groove. Therefore, it supports its diffusional heat transfer by advection and increases total convection of the first groove. Due to the stagnant like slow motion of the recirculation zone, heat is dissipated towards upstream through the recirculation zone up to the step by diffusion mostly.

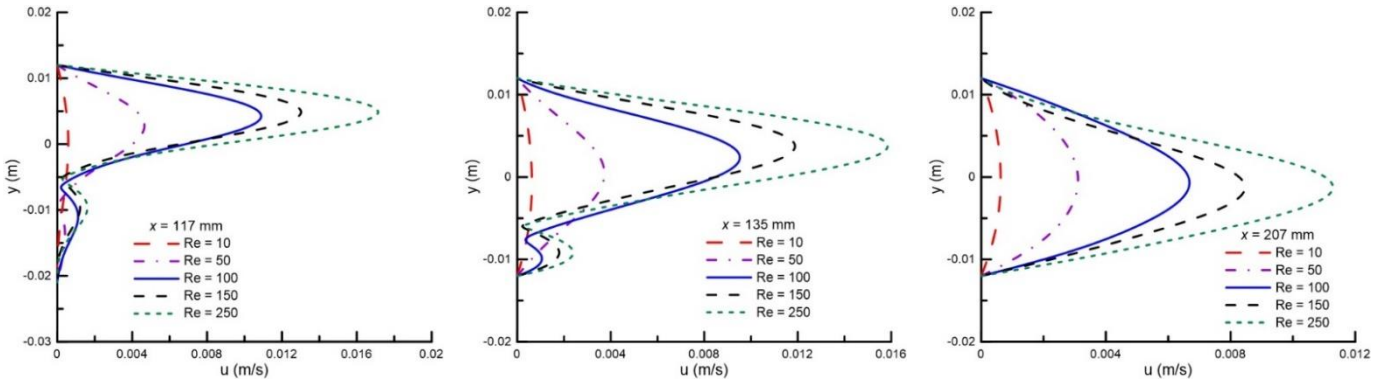

(a) Sampling point 1 (b) Sampling point 2 (c) Sampling point 3

Figure 6. Streamwise velocity component distribution on traverse lines (cross-stream) at three different sampling points depending on Re and φ

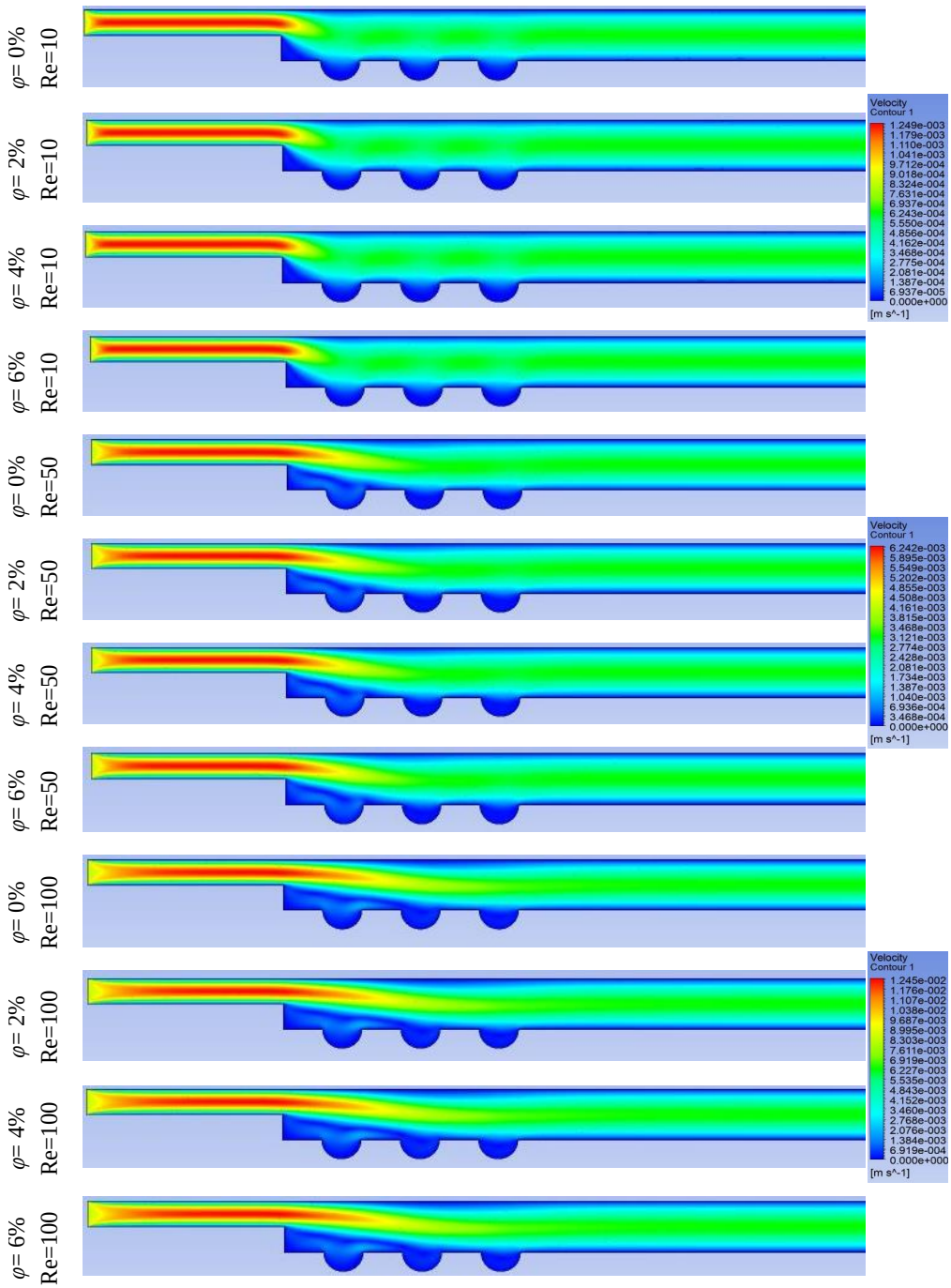

(a) Re=10, 50, 100

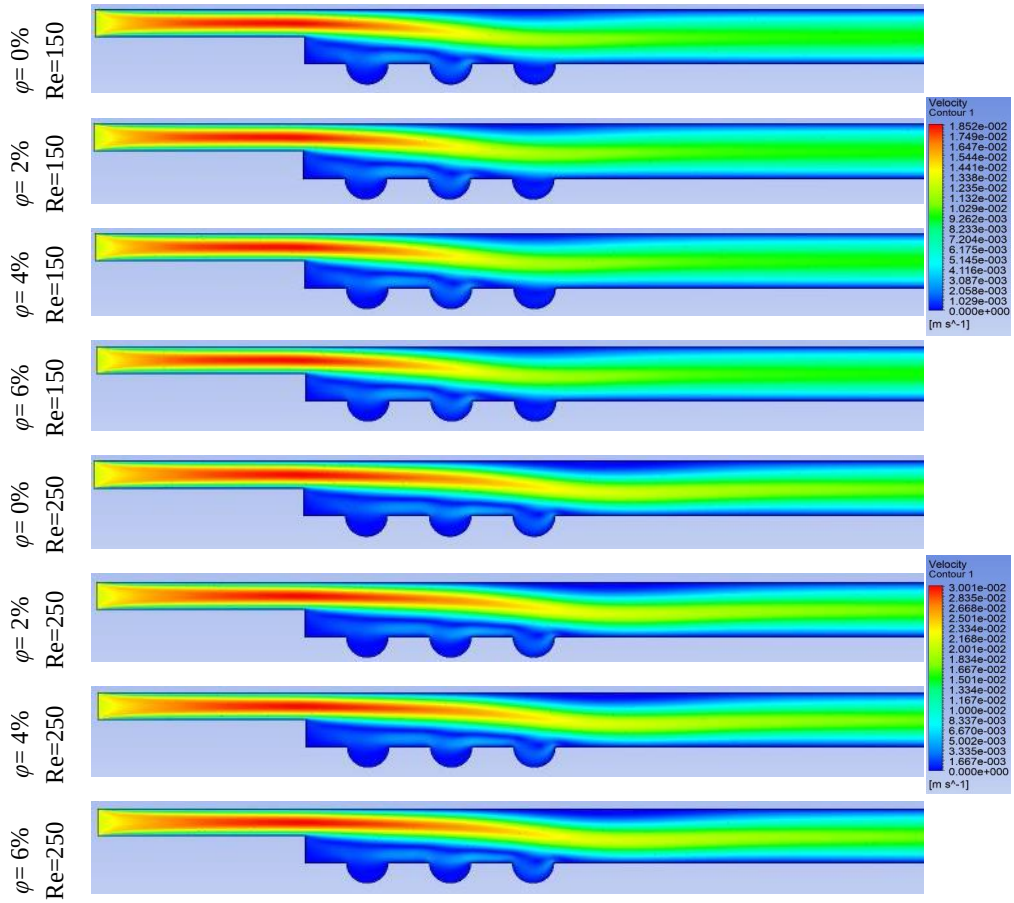

(b) Re=150, 250

Figure 7. Velocity distribution in the calculation domain according to Re=10, 50, 100, 150, 250 and nano particle volume fraction ratio

Remaining grooves transfer heat first by diffusion and then through laminar flow. Stagnant or slow flow near proximity of the bottom wall also transfers some amount of heat by almost pure diffusion. Accordingly, those proximities have higher temperature values. A small recirculation zone appears on the upper wall, but it is very weak and seems to have no effect on the flow and accordingly heat transfer. Core flow has higher maximum velocities comparing to Re=10. Re=100 changes flow structure a little bit more. The small recirculation zone of upper wall grows bigger with Re=100. This narrows the core flow between bottom and upper recirculation zones. Accordingly maximum velocity values of core flow reach more distances in streamwise direction. Relatively high velocity core flow entraps bottom recirculation zone from growing further and limits with the second groove downstream edge. Nevertheless, upper recirculation zone is still small, and its only effect is keeping core flow velocities high and hence bottom recirculation zone relatively small.

Bottom recirculation zone at Re=100 still strongly interacts with the first groove. This again increases convection in the first groove. The diffusion increases the temperature in bottom recirculation zone considering the temperature distribution graphics. The shear layer between core flow and bottom recirculation zone causes entrainment and heat exchange between higher temperature recirculation zone and lower temperature core flow. With Re=150, bottom recirculation zone starts to interact with the depths of the second groove. Therefore, one sees higher convection coefficient of the second groove surface. Recirculation motion seems to be leaving the first groove. This explains why thermal convection coefficient of the second groove is higher than the first groove. Core flow maximum velocity magnitudes reaches more distances in streamwise direction. This is partly due to growing upper recirculation zone. Finally, Re=250 velocity distribution graphics show that the responsible mechanism that drive interaction with grooves is the location of reattachment point. As the attachment point reaches to the depths of the third groove, a relatively more energetic motion occurs in the third groove increasing its thermal convection coefficient to the highest value. Upper recirculation zone grows to its maximum volume, leading to maximum velocity magnitudes in core flow to reach almost to the end of the third groove. The increased temperature values of the bottom recirculation zone due to thermal diffusion transfers heat to core flow through shear layer. Core flow temperature remains low because of its relatively high movement speed.

The final figure is for local Nu number at the grooves (Figure 8). Since all the surfaces are insulated except the surfaces of the grooves, total heat transferred into the calculation domain is through those surfaces. Accordingly, calculated local Nu numbers have very high values. The reason of lower average Nu numbers is due to zero values of local Nu numbers at adiabatic surfaces. The upstream edges of the grooves start with a moderate Nu number value about 125. Flow may be separated right after the upstream edge and therefore local Nu drops to about 100 value. Then local Nu increases up to 200 value as location approaches to the downstream edges of the grooves. The first groove local Nu is higher because of the previously explained recirculation zone interaction with the depths of the first groove.

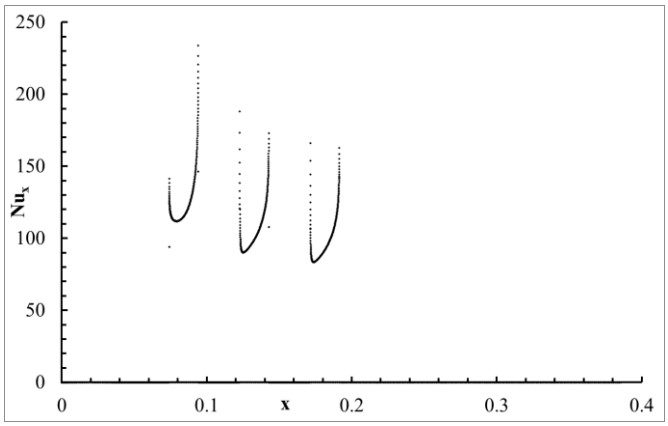

Figure 8. Local Nu inside the grooves at Re=100 and φ=6%

4. CONCLUSION

A two dimensional Back Facing Step (BFS) geometry is modified, and three circular grooves are placed downstream of the step. All surfaces except the groove surfaces are insulated. Five different laminar flow are used to investigate forced convection heat transfer case. Computational Fluid Dynamics (CFD) is used for the analysis. The investigated case is unique according to scientific literature and poses an interesting solution of partial heating problem. According to the literature survey, it is seen that solid surfaces and geometries are used in order to modify the BFS flow and thus heat transfer. There are few examples of partial heating. However, those examples are quite different from the present setup. The real-world implications in terms of industrial applications are that of cooling electronics where partial heat generation is subjected to BFS resembling flows.

It is seen that BFS recirculation zone strongly interact with grooves via its reattachment point, leading to a local heat transfer increase. The relatively slow and stagnant nature of the recirculation zone causes heat diffusion to move towards upstream through it up to the step. This is especially true by the contribution of nano particle fractions. As a major conclusion, structures to be cooled in the downstream of a BFS need to be carefully located considering present results. It can be stated that conduction in streamwise and cross-stream directions through the fluid domain is significant and strongly depends on nano-particle concentration in the nanofluid. One should consider peak temperature locations in an application bearing similar conditions with this case since regional peaks can be important in system operations, especially in electronics. Flow structure determines the trends and nano-particle concentrations determine the magnitude of heat transfer. Discrete Phase Model (DPM) can be used in future in order to resolve particle accumulation. Trade-off between heat transfer enhancement and pressure drop can be analysed in terms of energy and entropy generation.

ACKNOWLEDGMENT

Authors acknowledge the infrastructure of Selcuk University, University of Kirkuk, and Tikrit University in terms of software and literature databases.

REFERENCES

[1] Karasu, T. (2001). Geriye doğru basamaklar arkasında kompleks çevrintili türbülanslı akışın sayısal hesaplanmasıII Ulusal Hidrolik Pnömatik Kongresi. İzmir TURKEY, pp. 475-485.

[2] Yang, X.D., Ma, H.Y., Huang, Y.N. (2005). Prediction of homogeneous shear flow and a backward-facing step flow with some linear and non-linear K-ε turbulence models. Communications in Nonlinear Science and Numerical Simulation, 10(3): 315-328. https://doi.org/10.1016/j.cnsns.2003.07.001

[3] Almohammadi, K.M. (2020). Assessment of reattachment length using turbulence models on backward facing step (BFS) for turbulent flow with modified general Richardson method. Arabian Journal for Science and Engineering, 45(11): 9293-9303. https://doi.org/10.1007/s13369-020-04695-0

[4] Wang, W., Zhang, L., Yan, Y. (2012). Large eddy simulation of turbulent flow downstream of a backward-facing step. Procedia Engineering, 31: 16-22. https://doi.org/10.1016/j.proeng.2012.01.984

[5] Vogel, J. (1985). Combined heat transfer and fluid dynamic measurements downstream of a backward-facing Step. J. Heat Transfer, 107: 922-929.

[6] Assam, A., Kalkote, N., Dongari, N., Eswaran, V. (2019). Investigation of non-equilibrium boundary conditions considering sliding friction for micro/nano flows. International Journal of Numerical Methods for Heat & Fluid Flow, 29(8): 2501-2523. https://doi.org/10.1108/HFF-04-2018-0170

[7] Erturk, E. (2008). Numerical solutions of 2-D steady incompressible flow over a backward-facing step, Part I: High Reynolds number solutions. Computers & Fluids, 37(6): 633-655. https://doi.org/10.1016/j.compfluid.2007.09.003

[8] Armaly, B.F., Durst, F., Pereira, J.C.F., Schönung, B. (1983). Experimental and theoretical investigation of backward-facing step flow. Journal of Fluid Mechanics, 127: 473-496. https://doi.org/10.1017/S0022112083002839

[9] Nowruzi, H., Nourazar, S.S., Ghassemi, H. (2018). On the instability of two dimensional backward-facing step flow using energy gradient method. Journal of Applied Fluid Mechanics, 11(1): 241-256. https://doi.org/10.29252/jafm.11.01.28235

[10] Zhu, Y., Yi, S., Ding, H., Nie, W., Zhang, Z. (2019). Structures and aero-optical effects of supersonic flow over a backward facing step with vortex generators. European Journal of Mechanics-B/Fluids, 74: 302-311. https://doi.org/10.1016/j.euromechflu.2018.09.003

[11] Guo, G.M., Liu, H., Zhang, B. (2017). Numerical study of active flow control over a hypersonic backward-facing step using supersonic jet in near space. Acta Astronautica, 132: 256-267. https://doi.org/10.1016/j.actaastro.2016.12.035

[12] Dejoan, A., Leschziner, M.A. (2004). Large eddy simulation of periodically perturbed separated flow over a backward-facing step. International Journal of Heat and Fluid Flow, 25(4): 581-592. https://doi.org/10.1016/j.ijheatfluidflow.2004.03.004

[13] Kapiris, P.G., Mathioulakis, D.S. (2014). Experimental study of vortical structures in a periodically perturbed flow over a backward-facing step. International Journal

of Heat and Fluid Flow, 47: 101-112. https://doi.org/10.1016/j.ijheatfluidflow.2014.03.004
[14] Louda, P., Příhoda, J., Kozel, K., Sváček, P. (2013). Numerical simulation of flows over 2D and 3D backward-facing inclined steps. International Journal of Heat and Fluid Flow, 43: 268-276. https://doi.org/10.1016/j.ijheatfluidflow.2013.05.023
[15] Choi, H.H., Nguyen, J. (2016). Numerical investigation of backward facing step flow over various step angles. Procedia Engineering, 154: 420-425. https://doi.org/10.1016/j.proeng.2016.07.508
[16] Rouizi, Y., Girault, M., Favennec, Y., Petit, D. (2010). Model reduction by the Modal Identification Method in forced convection: Application to a heated flow over a backward-facing step. International Journal of Thermal Sciences, 49(8): 1354-1368. https://doi.org/10.1016/j.ijthermalsci.2010.02.011
[17] Terhaar, S., Velazquez, A., Arias, J.R., Sanchez-Sanz, M. (2010). Experimental study on the unsteady laminar heat transfer downstream of a backwards facing step. International Communications in Heat and Mass Transfer, 37(5): 457-462. https://doi.org/10.1016/j.icheatmasstransfer.2010.01.009
[18] Coskun, U.C., Cadirci, S., Gunes, H. (2021). Numerical investigation of active flow control on laminar forced convection over a backward facing step surrounded by multiple jets. Journal of Applied Fluid Mechanics, 14(2): 447-458. https://doi.org/10.47176/jafm.14.02.31680
[19] Kumar, A., Dhiman, A.K. (2012). Effect of a circular cylinder on separated forced convection at a backward-facing step. International Journal of Thermal Sciences, 52: 176-185. https://doi.org/10.1016/j.ijthermalsci.2011.09.014
[20] Xu, J.H., Zou, S., Inaoka, K., Xi, G.N. (2017). Effect of Reynolds number on flow and heat transfer in incompressible forced convection over a 3D backward-facing step. International Journal of Refrigeration, 79: 164-175. https://doi.org/10.1016/j.ijrefrig.2017.04.012
[21] Xie, W.A., Xi, G.N. (2017). Fluid flow and heat transfer characteristics of separation and reattachment flow over a backward-facing step. International Journal of Refrigeration, 74: 177-189. https://doi.org/10.1016/j.ijrefrig.2016.10.006
[22] Xie, W.A., Xi, G.N., Zhong, M.B. (2017). Effect of the vortical structure on heat transfer in the transitional flow over a backward-facing step. International Journal of Refrigeration, 74: 465-474. https://doi.org/10.1016/j.ijrefrig.2016.11.001
[23] Boruah, M.P., Randive, P.R., Pati, S. (2018). Hydrothermal performance and entropy generation analysis for mixed convective flows over a backward facing step channel with baffle. International Journal of Heat and Mass Transfer, 125: 525-542. https://doi.org/10.1016/j.ijheatmasstransfer.2018.04.094
[24] Selimefendigil, F., Öztop, H.F. (2017). Forced convection and thermal predictions of pulsating nanofluid flow over a backward facing step with a corrugated bottom wall. International Journal of Heat and Mass Transfer, 110: 231-247. https://doi.org/10.1016/j.ijheatmasstransfer.2017.03.010
[25] Selimefendigil, F., Öztop, H.F. (2013). Numerical analysis of laminar pulsating flow at a backward facing step with an upper wall mounted adiabatic thin fin. Computers & Fluids, 88: 93-107. https://doi.org/10.1016/j.compfluid.2013.08.013
[26] Selimefendigil, F., Öztop, H.F. (2013). Identification of forced convection in pulsating flow at a backward facing step with a stationary cylinder subjected to nanofluid. International Communications in Heat and Mass Transfer, 45: 111-121. https://doi.org/10.1016/j.icheatmasstransfer.2013.04.016
[27] Selimefendigil, F., Öztop, H.F. (2014). Effect of a rotating cylinder in forced convection of ferrofluid over a backward facing step. International Journal of Heat and Mass Transfer, 71: 142-148. https://doi.org/10.1016/j.ijheatmasstransfer.2013.12.042
[28] Selimefendigil, F., Öztop, H.F. (2015). Numerical investigation and reduced order model of mixed convection at a backward facing step with a rotating cylinder subjected to nanofluid. Computers & Fluids, 109: 27-37. https://doi.org/10.1016/j.compfluid.2014.12.007
[29] Velazquez, A., Arias, J.R., Mendez, B. (2008). Laminar heat transfer enhancement downstream of a backward facing step by using a pulsating flow. International Journal of Heat and Mass Transfer, 51(7-8): 2075-2089. https://doi.org/10.1016/j.ijheatmasstransfer.2007.06.009
[30] Juste, G.L., Fajardo, P. (2018). Influence of flow tree-dimensionality on the heat transfer of a narrow channel backward facing step flows. International Journal of Thermal Sciences, 132: 234-248. https://doi.org/10.1016/j.ijthermalsci.2018.06.005
[31] Sivasubramanian, M., Kanna, P.R., Uthayakumar, M., Ganesan, P. (2015). Experimental investigation on heat transfer enhancement from a channel mounted with staggered blocks. Arabian Journal for Science and Engineering, 40(4): 1123-1139. https://doi.org/10.1007/s13369-015-1570-8
[32] Li, Z.Y., Guo, S., Bai, H.L., Gao, N. (2019). Combined flow and heat transfer measurements of backward facing step flows under periodic perturbation. International Journal of Heat and Mass Transfer, 130: 240-251. https://doi.org/10.1016/j.ijheatmasstransfer.2018.10.077
[33] Chen, Y.T., Nie, J.H., Armaly, B.F., Hsieh, H.T. (2006). Turbulent separated convection flow adjacent to backward-facing step-effects of step height. International Journal of Heat and Mass Transfer, 49(19-20): 3670-3680. https://doi.org/10.1016/j.ijheatmasstransfer.2006.02.024
[34] Amiri, A., Arzani, H.K., Kazi, S.N., Chew, B.T., Badarudin, A. (2016). Backward-facing step heat transfer of the turbulent regime for functionalized graphene nanoplatelets based water-ethylene glycol nanofluids. International Journal of Heat and Mass Transfer, 97: 538-546. https://doi.org/10.1016/j.ijheatmasstransfer.2016.02.042
[35] Mittal, R., Madanan, U., Goldstein, R.J. (2017). The heat/mass transfer analogy for a backward facing step. International Journal of Heat and Mass Transfer, 113: 411-422. https://doi.org/10.1016/j.ijheatmasstransfer.2017.05.087
[36] Hilo, A.K., Iborra, A.A., Sultan, M.T.H., Hamid, M.F.A. (2020). Experimental study of nanofluids flow and heat transfer over a backward-facing step channel. Powder Technology, 372: 497-505. https://doi.org/10.1016/j.powtec.2020.06.013

[37] Hilo, A.K. (2021). Fluid flow and heat transfer over corrugated backward facing step channel. Case Studies in Thermal Engineering, 24: 100862. https://doi.org/10.1016/j.csite.2021.100862
[38] Chen, L., Asai, K., Nonomura, T., Xi, G., Liu, T. (2018). A review of Backward-Facing Step (BFS) flow mechanisms, heat transfer and control. Thermal Science and Engineering Progress, 6: 194-216. https://doi.org/10.1016/j.tsep.2018.04.004
[39] Montazer, E., Yarmand, H., Salami, E., Muhamad, M.R., Kazi, S.N., Badarudin, A. (2018). A brief review study of flow phenomena over a backward-facing step and its optimization. Renewable and Sustainable Energy Reviews, 82: 994-1005. https://doi.org/10.1016/j.rser.2017.09.104
[40] Abu-Mulaweh, H.I. (2005). Turbulent mixed convection flow over a forward-facing step-the effect of step heights. International Journal of Thermal Sciences, 44(2): 155-162. https://doi.org/10.1016/j.ijthermalsci.2004.08.001
[41] Öztop, H.F. (2006). Turbulence forced convection heat transfer over double forward facing step flow. International Communications in Heat and Mass Transfer, 33(4): 508-517. https://doi.org/10.1016/j.icheatmasstransfer.2005.08.015
[42] Nassab, S.G., Moosavi, R., Sarvari, S.H. (2009). Turbulent forced convection flow adjacent to inclined forward step in a duct. International Journal of Thermal Sciences, 48(7): 1319-1326. https://doi.org/10.1016/j.ijthermalsci.2008.10.003
[43] Oztop, H.F., Mushatet, K.S., Yılmaz, İ. (2012). Analysis of turbulent flow and heat transfer over a double forward facing step with obstacles. International Communications in Heat and Mass Transfer, 39(9): 1395-1403. https://doi.org/10.1016/j.icheatmasstransfer.2012.07.011
[44] Togun, H., Ahmadi, G., Abdulrazzaq, T., Shkarah, A.J., Kazi, S.N., Badarudin, A., Safaei, M.R. (2015). Thermal performance of nanofluid in ducts with double forward-facing steps. Journal of the Taiwan Institute of Chemical Engineers, 47: 28-42. https://doi.org/10.1016/j.jtice.2014.10.009
[45] Selimefendigil, F. (2013). Numerical analysis and pod based interpolation of mixed convection heat transfer in horizontal channel with cavity heated from below. Engineering Applications of Computational Fluid Mechanics, 7(2): 261-271. https://doi.org/10.1080/19942060.2013.11015469
[46] Mohammed, K.A., Talib, A.A., Nuraini, A.A., Ahmed, K.A. (2017). Review of forced convection nanofluids through corrugated facing step. Renewable and Sustainable Energy Reviews, 75: 234-241. https://doi.org/10.1016/j.rser.2016.10.067
[47] Rokita, T., Greenberg, J.B., Arieli, R., Levy, Y. (2018). Spatial-temporal patterns of three-dimensional subsonic turbulent cavity flow. International Journal of Heat and Fluid Flow, 71: 260-274. https://doi.org/10.1016/j.ijheatfluidflow.2018.04.004
[48] Yang, W.M., Chou, S.K., Shu, C., Li, Z.W., Xue, H. (2002). Combustion in micro-cylindrical combustors with and without a backward facing step. Applied Thermal Engineering, 22(16): 1777-1787. https://doi.org/10.1016/S1359-4311(02)00113-8
[49] Khandelwal, B., Deshpande, A.A., Kumar, S. (2013). Experimental studies on flame stabilization in a three step rearward facing configuration based micro channel combustor. Applied Thermal Engineering, 58(1-2): 363-368. https://doi.org/10.1016/j.applthermaleng.2013.04.058
[50] Choi, B.C., Ghoniem, A.F. (2018). Stabilization and blowout characteristics of lean premixed turbulent flames behind a backward-facing step in a rectangular combustor with heated propane-air mixtures. Fuel, 222: 627-637. https://doi.org/10.1016/j.fuel.2018.02.160
[51] Li, C., Chen, X., Li, Y., Musa, O., Zhu, L., Li, W. (2019). Role of the backward-facing steps at two struts on mixing and combustion characteristics in a typical strut-based scramjet with hydrogen fuel. International Journal of Hydrogen Energy, 44(52): 28371-28387. https://doi.org/10.1016/j.ijhydene.2019.09.023
[52] Aabid, A., Khan, S.A. (2021). Investigation of high-speed flow control from CD nozzle using design of experiments and CFD methods. Arabian Journal for Science and Engineering, 46(3): 2201-2230. https://doi.org/10.1007/s13369-020-05042-z
[53] Ghasemi, J., Razavi, S.E. (2013). Numerical nanofluid simulation with finite volume Lattice-Boltzmann enhanced approach. Journal of Applied Fluid Mechanics, 6(4): 519-527.
[54] Hernandez, A., Muñoz, R., Ventura, S., Büscher, W., Christoph, R. (2018). Study of low cost materials for the enhancement of solar seawater desalination. Periodico Tche Quimica, 15(29): 300-308.
[55] Amorim Neto, J.P.D., Pontes, R.J., Rocha, P.A.C., Marinho, F.P., da Silva, M.E. (2020). Experimental analysis of a solar heat system using hybrid silver nano fluid and titanium dioxide. Periodico Tche Quimica, 17(34): 448-458. https://doi.org/10.52571/PTQ.v17.n34.2020.472_P34_pgs_448_458.pdf
[56] Khodabandeh, E., Toghraie, D., Chamkha, A., Mashayekhi, R., Akbari, O., Rozati, S.A. (2019). Energy saving with using of elliptic pillows in turbulent flow of two-phase water-silver nanofluid in a spiral heat exchanger. International Journal of Numerical Methods for Heat & Fluid Flow, 30(4): 2025-2049. https://doi.org/10.1108/HFF-10-2018-0594
[57] Selimefendigil, F., Chamkha, A. J. (2019). Cooling of an isothermal surface having a cavity component by using CuO-water nano-jet. International Journal of Numerical Methods for Heat & Fluid Flow, 30(4): 2169-2191. https://doi.org/10.1108/HFF-12-2018-0724
[58] Abedalh, A.S., Shaalan, Z.A., Yassien, H.N.S. (2021). Mixed convective of hybrid nanofluids flow in a backward-facing step. Case Studies in Thermal Engineering, 25: 100868. https://doi.org/10.1016/j.csite.2021.100868
[59] Abed, N., Afgan, I., Cioncolini, A., Iacovides, H., Nasser, A., Mekhail, T. (2020). Thermal performance evaluation of various nanofluids with non-uniform heating for parabolic trough collectors. Case Studies in Thermal Engineering, 22: 100769. https://doi.org/10.1016/j.csite.2020.100769
[60] Ahmed, M.A., Yaseen, M.M., Yusoff, M.Z. (2017). Numerical study of convective heat transfer from tube bank in cross flow using nanofluid. Case Studies in Thermal Engineering, 10: 560-569.

https://doi.org/10.1016/j.csite.2017.11.002
[61] Ahmed, M.A., Yusoff, M.Z., Ng, K.C., Shuaib, N.H. (2014). The effects of wavy-wall phase shift on thermal-hydraulic performance of Al_2O_3–water nanofluid flow in sinusoidal-wavy channel. Case Studies in Thermal Engineering, 4: 153-165. https://doi.org/10.1016/j.csite.2014.09.005
[62] Ajeel, R.K., Salim, W.I., Hasnan, K. (2018). Thermal and hydraulic characteristics of turbulent nanofluids flow in trapezoidal-corrugated channel: Symmetry and zigzag shaped. Case Studies in Thermal Engineering, 12: 620-635. https://doi.org/10.1016/j.csite.2018.08.002
[63] Hechavarria, R., Delgado, O., Hidalgo, A., Segundo, E., Guamanquispe, J. (2018). Photothermal technique for measuring thermal conductivity and diffusivity of nanofluids: a new approach. Periódico Tchê Química, 15(29): 257-265.
[64] Rocha, P.A.C., Santos, R.F.D.M., Lima, R.J.P., da Silva, M.E.V. (2019). A review on nanofluids: preparation methods and applications. Periodico Tche Quimica, 16(31): 365-380.
[65] Al-Aswadi, A.A., Mohammed, H.A., Shuaib, N.H., Campo, A. (2010). Laminar forced convection flow over a backward facing step using nanofluids. International Communications in Heat and Mass Transfer, 37(8): 950-957. https://doi.org/10.1016/j.icheatmasstransfer.2010.06.007
[66] Mohammed, H.A., Gunnasegaran, P., Shuaib, N.H. (2011). The impact of various nanofluid types on triangular microchannels heat sink cooling performance. International Communications in Heat and Mass Transfer, 38(6): 767-773. https://doi.org/10.1016/j.icheatmasstransfer.2011.03.024
[67] Canli, E., Ali, A.T.E.S., & Bilir, Ş. (2020). Derivation of dimensionless governing equations for axisymmetric incompressible turbulent flow heat transfer based on standard k-ϵ model. Afyon Kocatepe Üniversitesi Fen Ve Mühendislik Bilimleri Dergisi, 20(6): 1096-1111. https://doi.org/10.35414/akufemubid.821009
[68] Bilir, Ş., Ateş, A. (2003). Transient conjugated heat transfer in thick walled pipes with convective boundary conditions. International Journal of Heat and Mass Transfer, 46(14): 2701-2709. https://doi.org/10.1016/S0017-9310(03)00032-2

NOMENCLATURE

A	area (m^2)
c_p	specific energy at constant pressure (J/kg·K)
$\mathbf{f}$	body forces vector (N)
h	thermal convection coefficient ($W/m^2 \cdot K$)
H	channel height (m)
k	thermal conductivity (W/m·K)
p	pressure (Pa)
P	nondimensionalized pressure
$\dot{q}$	heat flux (W/m^2)
t	time (s)
T	temperature (K)
u	streamwise velocity (m/s)
U	dimensionless streamwise velocity
v	cross-stream velocity (m/s)
$\mathbf{v}$	Velocity vector (m/s)
V	dimensionless cross-stream velocity
x	x direction (m)
X	dimensionless x direction
y	y direction (m)
Y	dimensionless y direction
∇	vector del operator
φ	nano particle volume fraction (%)
μ	dynamic viscosity (kg/m·s)
ρ	density (kg/m^3)
$\boldsymbol{\tau}$	stress tensor (Pa)
θ	dimensionless temperature

Subscripts

bf	base fluid
nf	nanofluid
in	inlet
p	nano particle
s	surface
v	volume